

Improvement of a focused ion beam fabricated diamond pillar for scanning ensemble nitrogen-vacancy magnetometry probe using an ultrapure diamond

Dwi Prananto^{1*}, Yifei Wang¹, Yuta Kainuma^{1†}, Kunitaka Hayashi¹, Masahiko Tomitori¹, and Toshu An^{1‡}

¹*School of Materials Science, Japan Advanced Institute of Science and Technology, Nomi, Ishikawa 923-1292, Japan*

*E-mail: prananto@jaist.ac.jp

†Present address: *Global Research and Development Center for Business by Quantum-AI technology (G-QuAT), National Institute of Advanced Industrial Science and Technology (AIST), Tsukuba, Ibaraki, 305-8560, Japan*

‡E-mail: toshuan@jaist.ac.jp

Scanning diamond nitrogen-vacancy probe microscopy (SNVM) is an important tool for studying nanoscale condensed-matter phenomena. Ga⁺-ion-focused-ion-beam (FIB) milling has been introduced as an available method for fabricating SNVM, while the probe diameter is limited to a few micrometers due to the Ga⁺-induced damage. We report a method for improving the SNVM probes' quality, with an 800-nm diameter probe of ultrapure diamond, through polyvinyl alcohol and Pt/Pd capping, followed by UV/ozone exposure. The effectiveness of the method is confirmed by NVs' spin-coherence property measurements and magnetic domain structure imaging with a few-hundred-nanometer resolution and a 6.7 $\mu\text{T}/\text{Hz}^{1/2}$ sensitivity.

Since its invention in 1982, scanning probe microscopy (SPM)¹⁾ has played an indispensable role in studying physical and biological phenomena at the nanoscale²⁾. The technique has been further developed to include nanoscale sensors attached to the tip apex of an SPM probe, enabling various functionalities and purposes. Among them are the nitrogen-vacancy (NV) centers in diamond³⁾ (Fig. 1(a)), a multimodal quantum sensor based on optically addressable spin-triplet ($S = 1$) states⁴⁾ used for high-sensitivity and high-resolution sensing applications such as nanoscale magnetic domain structure imaging⁵⁾, nanoscale NMR⁶⁾, and temperature sensing of biological cells⁷⁾.

Recently, scanning diamond NV probe microscopy (SNVM) in the form of a diamond cantilever with a tip containing NV centers has been made possible by electron beam lithography and reactive ion etching⁸⁾, and is available commercially, e.g., Qnami AG and Qzabre AG⁹⁾. Ga⁺ ion-focused ion beam (FIB) has been used as an alternative method for diamond nanofabrication^{10),11)} and has recently been used to fabricate an SNVM probe from a type-IIa diamond¹²⁾. However, the probe tip diameter was limited to a few μm because of FIB-induced damage to the diamond^{13),14)}.

To mitigate the FIB-induced damage, here we introduce a method to preserve the near-surface ensemble of NV centers in an ultrapure diamond by capping with protective layers of polyvinyl alcohol (PVA) and Pt/Pd, followed by post-fabrication of ultraviolet (UV)/ozone surface treatment. The effectiveness of the treatment is evaluated by measuring the SNVM probe's spin properties before and after FIB fabrication, indicating that the spin properties are preserved.

An electronic grade (100)-oriented type-IIa diamond (Element Six) (measured $2 \times 2 \times 0.5 \text{ mm}^3$), with initial impurity of N < 5 ppb and B < 1 ppb, was polished to be 50 μm in thickness. The diamond was then implanted with ¹⁴N⁺ at the energy of 30 keV and a dosage of $1 \times 10^{12} \text{ ions/cm}^2$ and annealed at 900 °C for 1 hour under an Ar atmosphere to form a layer of NV centers at a mean depth of 40 nm (based on Monte Carlo simulation by SRIM¹⁵⁾). Next, the diamond was acid-cleaned using a 1:3 mixture of HNO₃ and H₂SO₄ at 220°C for 30 minutes and washed with deionized water. The diamond was then cut into triangular shapes by SYNTEK Co. Ltd using a laser beam. A triangular-shaped diamond was then picked up using a 30 μm diameter of electrochemically-sharpened tungsten probe operated via a micromanipulator arm (Micro Support Co. Ltd.) and placed on an acetone-dissolved acrylonitrile butadiene styrene (ABS) substrate. The diamond was pushed against the dissolved ABS, acting as a binder for the micrometer-sized amorphous carbon residue formed on the diamond surface after the laser-cut process¹⁶⁾, thereby recovering a clean diamond surface (Fig. 2(a), upper left). The diamond was then transferred and

fixed to a glass substrate using a fluoroelastomer adhesive (x-71-6046, Shin-Etsu) (Fig. 2(a) upper left).

Ga^+ ions FIB-milled on a diamond at 30 keV acceleration energy are known to create 30 nm-thick amorphous carbon residues and surface defects on the diamond, detrimental to the charge stability and coherence time of the NV centers^{13),14)}. Moreover, the FIB-milled diamond area is known to emit background fluorescence that may degrade the PL contrast of NV centers' optically detected magnetic resonance (ODMR)^{11),17),18)}. To protect the shallow NV centers from damage by Ga^+ ions and sample charging during the FIB milling process, the diamond was masked with a layer of polyvinyl alcohol (PVA) and subsequently with 160 nm Pt/Pd.

The SNVM probe was fabricated by a 30 keV Ga^+ ion beam in an FIB apparatus (SMI3050, SII NanoTechnology). The fabrication process was initialized by forming a square island of $7 \times 7 \times 5 \mu\text{m}^3$ using a rectangular milling pattern with 13 μA Ga^+ ion current to etch the area outside the square island. Next, a doughnut-shaped milling pattern of 7 μm outer diameter and 1 μm inner diameter was used to fabricate a 1.6 μm height pillar using a 720 pA Ga^+ ion current¹²⁾ (Fig. 2(a), upper-right panel). After fabrication, the diamond was soaked in a hot (60 °C) aqua regia solution (1:3 mixture of HCl: HNO_3) for 15 minutes to etch the Pt/Pd and PVA coatings, followed by 3 minutes of deionized water dipping (Fig. 2(a)). The SEM images in Fig. 1(c)-(d) show that the fabricated tip diameter was 800 nm.

After the fabrication process, we exposed the SNVM probe to UV/ozone to remove organic adsorbate and oxygen-terminate the surface¹⁹⁾⁻²⁴⁾. The UV/ozone treatment was performed at room temperature and oxygen pressure of 0.1 MPa using a UV/ozone cleaner (UV253, Nippon Laser and Electronics Laboratory).

After the UV/ozone treatment, the diamond was mechanically detached from the glass substrate and picked up using the manipulator to be mounted at the apex of another 30 μm -diameter electrochemically-sharpened tungsten rod attached to one prong of a quartz tuning fork (QTF) (Fig. 1(a)). The diamond was glued with silver paste (H20E, EPOTEK) and reinforced by epoxy glue (H74, EPOTEK). The SNVM probe was evaluated using a home-built scanning confocal microscopy (SCM) system consisting of a 532 nm laser source (MGL-III-532-80mW, Changchun New Industries Optoelectronics Technologies Co., Ltd.) guided through a 2D Galvano mirror system (GVS002, Thorlabs) to an objective lens (M Plan Apo 100 \times NA = 0.7, Mitutoyo) and focused on the tip of the SNVM probe. The laser polarized the NV center spins to the $m_s = 0$ state,

emitting photoluminescence (PL) at 600–800 nm detected with an avalanche photodiode (SCPM-ARQH-14FC, Excelitas Technologies) through the same objective lens. A laser scan over an area around the SNVM probe reconstructed a PL image of the probe (Fig. 2(b)). Note that there were no differences in PL intensity measured from the top and bottom (the probe tip side) of the diamond probe. A continuous-wave laser and microwave (SG6000F, DS Instruments) frequency sweep around 2.87 GHz resulted in an ODMR spectrum with a dip at 2.87 GHz at zero field (Fig. 2(c)). The PL Z-depth profile from the SNVM probe showed a full-width half-maximum of 2.3 μ m, comparable to the 2.2 μ m Z-axial diffraction limit of the objective lens (Fig. 2(d)), confirming the near-surface distribution of the NV centers in the ultrapure diamond as compared to the broadly distributed NV centers in our previously fabricated SNVM probe¹².

The home-built SCM system was combined with a QTF-based phase-locked loop (PLL)-regulated AFM system to form an integrated SNVM system. The AFM system consisted of XYZ piezo translation motors (ANPx101 and ANPz101, Attocube Systems) for coarse probe movement and an XYZ piezo tube scanner for moving the sample relative to the probe. An FPGA system (USB-7845R, National Instruments) controlled the integrated AFM system. The tip of the diamond probe was brought into proximity to the sample by the Z-axis piezo tube scanner. The horizontally-oscillating QTF was maintained in resonance by the PLL and provided an amplitude signal to feedback-control the tip-sample distance. The tip-sample distance was maintained, while the XY piezo tube scanner translated the sample to provide spatial information.

We evaluated the probe's spin coherence properties under a 10 mT external magnetic field aligned with one of the NV axes (<111> crystal-axis family). First, we checked the Rabi oscillation contrast ($m_s = 0 \leftrightarrow m_s = -1$) of the NV centers over an extended period of UV/ozone exposure. The Rabi oscillation was observed using a pulse protocol consisting of a 4 μ s polarizing laser pulse (Pol.), followed by a resonant microwave pulse of varying duration and a subsequent 4 μ s read-out laser pulse (RO1). An identical pulse sequence without MW provided a reference signal (RO2) for normalization (upper part of Fig. 3(a)).

The Rabi oscillation contrast, defined as the contrast between the maximum and minimum of the damped oscillation fit of the Rabi oscillation signals, was observed to be preserved at around 2 % (Fig. 3(b)). Spin coherence properties of a separate electronic grade diamond NV, prepared by the same implantation conditions of energy and dose and the post-NV generation surface acid treatment, were also measured and used as a control sample (referred as acid treatment dotted lines

in Fig. 3). In comparison to the control sample, the Rabi contrast post UV/ozone treatment was observed to be improved by about 1.5 times. In all Rabi oscillation experiments, the microwave power was adjusted to produce a Rabi oscillation frequency of ≈ 1.3 MHz. The improvement of Rabi oscillation contrast was possibly attributed to improving the diamond surface by oxygen termination, which suppressed the upward band bending of the valence band maximum of the diamond NV centers, as described by Yamano et al.²⁰.

The coherence times of the NV spins were inferred through the optical Hahn echo protocol with a MW sequence of $\pi/2 - \tau - \pi - \tau - \pi/2$ ($3\pi/2$) (upper part of Fig. 3(c)). The last MW pulse was altered between $\pi/2$ and $3\pi/2$ to rotate the superposition of $m_s = 0$ and $m_s = -1$ to respectively $m_s = 0$ (RO1) and $m_s = -1$ (RO2), to cancel common noise by subtracting RO1 and RO2. The longitudinal spin relaxation T_1 was evaluated by measuring the longitudinal spin relaxation of $m_s = 0$ and $m_s = -1$ (MW π -pulse) to their thermal equilibrium and subtracting the corresponding readout (RO1 and RO2, respectively) (upper part of Fig. 3(e)).

The coherence time T_2 Hahn echo of the fabricated SNVM probe was unchanged before and after the FIB fabrication process, followed by UV/ozone treatments, at the value of (30.4 ± 3.6) μ s (Fig. 3(d)). This is reasonable, considering the T_2 Hahn echo is limited dominantly by the bulk paramagnetic substitutional nitrogen (P1 center) created after the ion implantation, and is less sensitive to the surface paramagnetic defect species²⁵⁾⁻²⁷.

On the other hand, the T_1 was improved from (0.72 ± 0.015) ms before UV/ozone treatment to (1.83 ± 0.52) ms after 6 hours of UV/ozone treatment, comparable to the T_1 figure of (1.81 ± 0.31) ms of acid-treated diamond NV (Fig. 3(f)). T_1 with UV/ozone exposure can be seen as the result of the improved surface state of the diamond where the surface of the diamond, importantly around the rim of the diamond pillar, was terminated by a C–O–H group that significantly reduced the FIB-induced damage states near the surface of the diamond, leading to the reduction of paramagnetic noise on the surface of the diamond^{24),28}.

Finally, we demonstrated the applicability of the 800 nm-diameter SNVM probe for imaging the magnetic domain structure in a ferrimagnetic garnet, $(\text{BiLu})_3\text{Fe}_5\text{O}_{12}$ (BiLuIG). BiLuIG has in-plane magnetization and exhibits a magnetic domain structure at zero field with Néel-type domain walls²⁹). The sample was scanned over an area of 17.5×17.5 μm^2 (256×256 pixels) while pointing a continuous-wave laser on the NV centers probe and monitoring the PL. Fig. 4(a) shows the PL map showing the BiLuIG magnetic domain structure presented as bright areas with dark narrow

lines structure (Fig. 4(b)). The PL imaging is possible due to the presence of stray magnetic fields from the BiLuIG, where stray field vectors with a high off-axis to the NV spins' quantization axis [111] quench the PL emitted by the NV spins^{30),31)}. The dark lines in the PL image probably indicated the domain wall structure, which had a width of about 300 nm, inferred from the line cut of the periodic structure in the PL image (Fig. 4(b)). The domain wall width agrees with the estimated value of 400 nm based on the relation $\delta = \pi\sqrt{A/K_c}$, with $A = 3.7 \text{ pJ/m}$ as the exchange coupling constant and $K_c = 180 \text{ J/m}^3$ as the cubic anisotropy of BiLuIG²⁹⁾. The estimated DC magnetic field sensitivity based on the slope of the ODMR, in contact with the magnetic materials and zero magnetic bias field, was as small as $6.7 \mu\text{T/Hz}^{1/2}$.

In summary, we fabricated an SNVM probe using a laser cutting technique and Ga^+ ion FIB milling on an ultrapure diamond. We introduced a method for preserving the shallow NV center by PVA and Pt/Pd capping, followed by a room-temperature UV/ozone treatment, to mitigate the FIB-induced damage. Our SNVM probe preparation method preserved Rabi oscillation contrast and T_2 , and recovers T_1 after a few hours of UV/ozone treatment. The SNVM probe was tested to image the magnetic domain structure in a ferrimagnetic BiLuIG and resolved the 300 nm domain wall structure. In the future, it is worth investigating how lower-acceleration energy (<30 keV) of Ga^+ ion FIB milling suppresses the formation of the amorphous carbon layer and fabricates smaller-diameter probes (less than 200 nm) for higher-resolution condensed matter microscopy applications.

Acknowledgment

We thank N. Ito for the support in ion implantation, M. Ito for assisting with the FIB fabrication, and A. M. A. Hassan for the assistance in UV/ozone treatment. This work was supported, in part, by the JSPS KAKENHI Grant Nos. 24K01286 and 24K17580.

References

- 1) G. Binnig, H. Rohrer, Ch. Gerber and E. Weibel, Phys. Rev. Lett. **49** [1], 57 (1982).
- 2) K. Bian, C. Gerber, A. J. Heinrich, D. J. Müller, S. Scheuring and Y. Jiang, Nat. Rev. Methods Primer **1** [1], 36 (2021).
- 3) M. W. Doherty, N. B. Manson, P. Delaney, F. Jelezko, J. Wrachtrup and L. C. L. Hollenberg, Phys. Rep. **528** [1], 1 (2013).
- 4) R. Schirhagl, K. Chang, M. Loretz and C. L. Degen, Annu. Rev. Phys. Chem. **65** [1], 83 (2014).

5) L. Thiel, Z. Wang, M. A. Tschudin, D. Rohner, I. Gutiérrez-Lezama, N. Ubrig, M. Gibertini, E. Giannini, A. F. Morpurgo and P. Maletinsky, *Science* **364** [6444], 973 (2019).

6) D. B. Bucher, D. P. L. Aude Craik, M. P. Backlund, M. J. Turner, O. Ben Dor, D. R. Glenn and R. L. Walsworth, *Nat. Protoc.* **14** [9], 2707 (2019).

7) Y. Wu, F. Jelezko, M. B. Plenio and T. Weil, *Angew Chem Int Ed* **13** (2016).

8) P. Maletinsky, S. Hong, M. S. Grinolds, B. Hausmann, M. D. Lukin, R.-L. Walsworth, M. Loncar and A. Yacoby, *Nat. Nanotechnol.* **7** [5], 320 (2012).

9) See <https://qnami.ch/> for Qnami AG and <https://qzabre.com/> for QZabre AG.

10) J. P. Hadden, J. P. Harrison, A. C. Stanley-Clarke, L. Marseglia, Y.-L. D. Ho, B. R. Patton, J. L. O'Brien and J. G. Rarity, *Appl. Phys. Lett.* **97** [24], 241901 (2010).

11) M. Jamali, I. Gerhardt, M. Rezai, K. Frenner, H. Fedder and J. Wrachtrup, *Rev. Sci. Instrum.* **85** [12], 123703 (2014).

12) Y. Kainuma, K. Hayashi, C. Tachioka, M. Ito, T. Makino, N. Mizuochi and T. An, *J. Appl. Phys.* **130** [24], 243903 (2021).

13) I. Bayn, A. Bolker, C. Cytermann, B. Meyler, V. Richter, J. Salzman and R. Kalish, *Appl. Phys. Lett.* **99** [18], 183109 (2011).

14) S. Rubanov, A. Suvorova, V. P. Popov, A. A. Kalinin and Yu. N. Pal'yanov, *Diam. Relat. Mater.* **63**, 143 (2016).

15) J. F. Ziegler, M. D. Ziegler and J. P. Biersack, *Nucl. Instrum. Methods Phys. Res. Sect. B Beam Interact. Mater. At.* **268** [11–12], 1818 (2010).

16) K. S. Park and J. R. Youn, *Carbon* **50** [6], 2322 (2012).

17) Q. Jiang, D. Liu, G. Liu, Y. Chang, W. Li, X. Pan and C. Gu, *J. Appl. Phys.* **116** [4], 044308 (2014).

18) L. Marseglia, J. P. Hadden, A. C. Stanley-Clarke, J. P. Harrison, B. Patton, Y.-L. D. Ho, B. Naydenov, F. Jelezko, J. Meijer, P. R. Dolan, J. M. Smith, J. G. Rarity and J. L. O'Brien, *Appl. Phys. Lett.* **98** [13], 133107 (2011).

19) L. M. Apátiga and V. M. Castaño, *Appl. Phys. Lett.* **83** [22], 4542 (2003).

20) H. Yamano, S. Kawai, K. Kato, T. Kageura, M. Inaba, T. Okada, I. Higashimata, M. Haruyama, T. Tanii, K. Yamada, S. Onoda, W. Kada, O. Hanaizumi, T. Teraji, J. Isoya and H. Kawarada, *Jpn. J. Appl. Phys.* **56** [4S], 04CK08 (2017).

21) W. Kulisch, C. Popov, D. Gilliland, G. Ceccone, F. Rossi and J. P. Reithmaier, *Surf. Interface Anal.* **42** [6–7], 1152 (2010).

22) T. Sakai, K.-S. Song, H. Kanazawa, Y. Nakamura, H. Umezawa, M. Tachiki and H. Kawarada, *Diam. Relat. Mater.* **12** [10–11], 1971 (2003).

23) L. Rondin, G. Dantelle, A. Slablab, F. Grosshans, F. Treussart, P. Bergonzo, S. Perruchas, T. Gacoin, M. Chaigneau, H.-C. Chang, V. Jacques and J.-F. Roch, *Phys. Rev. B* **82** [11], 115449 (2010).

24) C. Li, X. Zhang, E. F. Oliveira, A. B. Puthirath, M. R. Neupane, J. D. Weil, A. G. Birdwell, T. G. Ivanov, S. Kong, T. Gray, H. Kannan, A. Biswas, R. Vajtai, D. S. Galvao and P. M. Ajayan, *Carbon* **182**, 725 (2021).

25) J.-P. Tetienne, R. W. de Gille, D. A. Broadway, T. Teraji, S. E. Lillie, J. M. McCoey, N. Dotschuk, L. T. Hall, A. Stacey, D. A. Simpson and L. C. L. Hollenberg, *Phys. Rev. B* **97** [8], 085402 (2018).

26) E. Bauch, S. Singh, J. Lee, C. A. Hart, J. M. Schloss, M. J. Turner, J. F. Barry, L. M. Pham, N. Bar-Gill, S. F. Yelin and R. L. Walsworth, *Phys. Rev. B* **102** [13], 134210 (2020).

27) H. Park, J. Lee, S. Han, S. Oh and H. Seo, *Npj Quantum Inf.* **8** [1], 95 (2022).

28) S. Sangtawesin, B. L. Dwyer, S. Srinivasan, J. J. Allred, L. V. H. Rodgers, K. De Greve, A. Stacey, N. Dontschuk, K. M. O'Donnell, D. Hu, D. A. Evans, C. Jaye, D. A. Fischer, M. L. Markham, D. J. Twitchen, H. Park, M. D. Lukin and N. P. de Leon, *Phys. Rev. X* **9** [3], 031052 (2019).

29) T. Hioki, R. Tsuboi, T. H. Johansen, Y. Hashimoto and E. Saitoh, *Appl. Phys. Lett.* **116** [11], 112402 (2020).

30) J.-P. Tetienne, L. Rondin, P. Spinicelli, M. Chipaux, T. Debuisschert, J.-F. Roch and V. Jacques, *New J. Phys.* **14** [10], 103033 (2012).

31) L. Rondin, J.-P. Tetienne, P. Spinicelli, C. Dal Savio, K. Karrai, G. Dantelle, A. Thiaville, S. Rohart, J.-F. Roch and V. Jacques, *Appl. Phys. Lett.* **100** [15], 153118 (2012).

Figures and captions

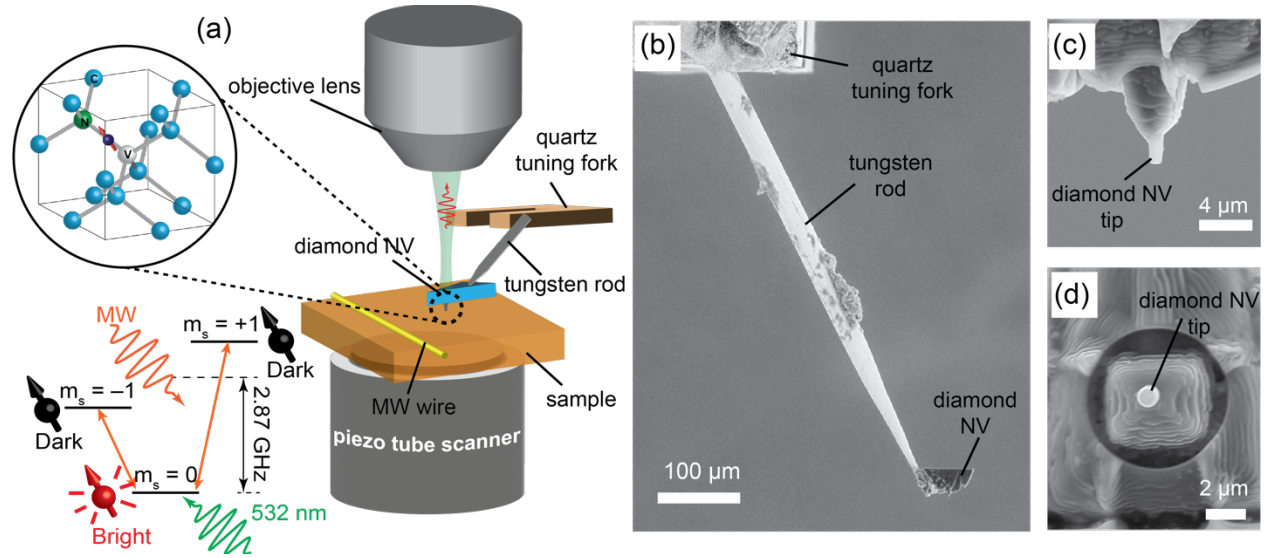


Fig. 1. (a) An FIB-fabricated SNVM probe was attached to the tip of a tungsten rod mounted on one prong of the quartz tuning fork, which was part of an integrated AFM system combined with a confocal microscopy system. (b) SEM image of the diamond NV probe attached to a tungsten rod. (c) Enlarged SEM image of the diamond NV probe showing the FIB-fabricated tip. (d) Same as (c) as seen from the bottom.

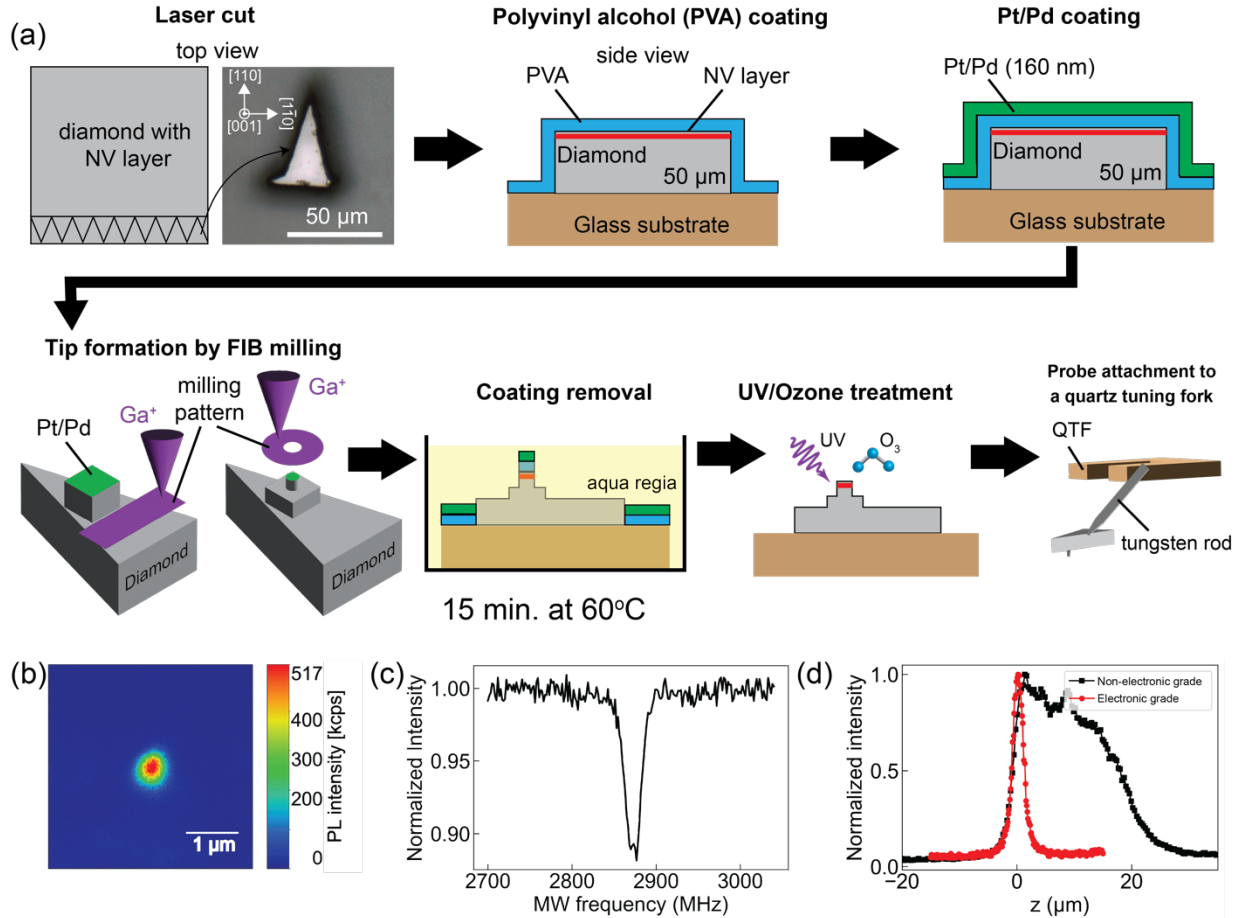


Fig. 2. (a) An SNVM probe fabrication process. A 50 μm thick diamond with an NV layer at 40 nm underneath its surface was cut into triangular shapes. A triangular-shaped diamond was picked up and masked with polyvinyl alcohol (PVA) and Pt/Pd (160 nm). The diamond was then milled with Ga⁺ FIB to fabricate a pillar with a height of 1.6 μm and a diameter of 800 nm. The diamond was then dipped into a hot (60 °C) aqua regia for 15 minutes, followed by a DI water dip. Before being attached to a tungsten rod, the surface of the diamond probe was treated with UV/ozone exposure. (b) PL image of the SNVM tip. (c) The ODMR of the NV spins in the SNVM probe at zero external magnetic field, showing a drop in PL intensity at 2.87 GHz. (d) PL depth profile of NV diamonds produced in a non-electronic grade (black square) and an electronic grade (red circle) type IIa diamonds. FWHM of the electronic grade PL depth was 2.3 μm and 19 μm for the non-electronic grade diamond. Solid lines are a guide to the eyes.

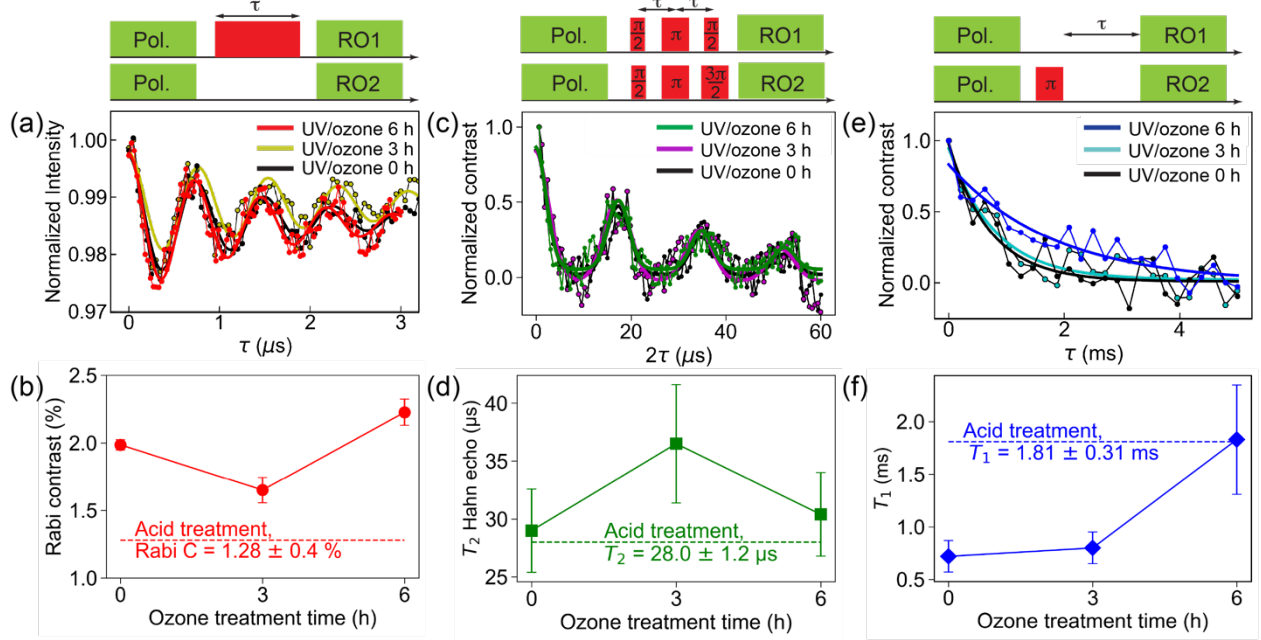


Fig. 3. (a) Rabi oscillation of the SNVM probe before (solid-black line), after 3 h (solid dark-yellow line), and after 6 h (solid-red line) of UV/ozone exposure. (b) Rabi oscillation contrast as a function of UV/ozone exposure time. (c) Hahn echo of the SNVM probe before (solid black line), after 3 h (solid-green line), and after 6 h (solid-green line) of UV/ozone exposure. (d) Hahn echo T_2 as a function of UV/ozone treatment time. The T_2 Hahn echo value before FIB fabrication (acid treatment) is shown as a dashed green line. (e) Longitudinal spin relaxation of the SNVM probe before (solid-black line), after 3 h (solid-cyan line), and after 6 h (solid-blue line) of UV/ozone exposure. (f) Longitudinal relaxation T_1 with increasing UV/ozone exposure time. The T_1 value before FIB fabrication (acid treatment) is shown as a solid blue line. Solid lines in (a), (c), and (e) are fitting lines, and solid lines in (b), (d), and (f) are a guide to the eyes. Error bars represent the standard deviation of the fitting to the experimental data.

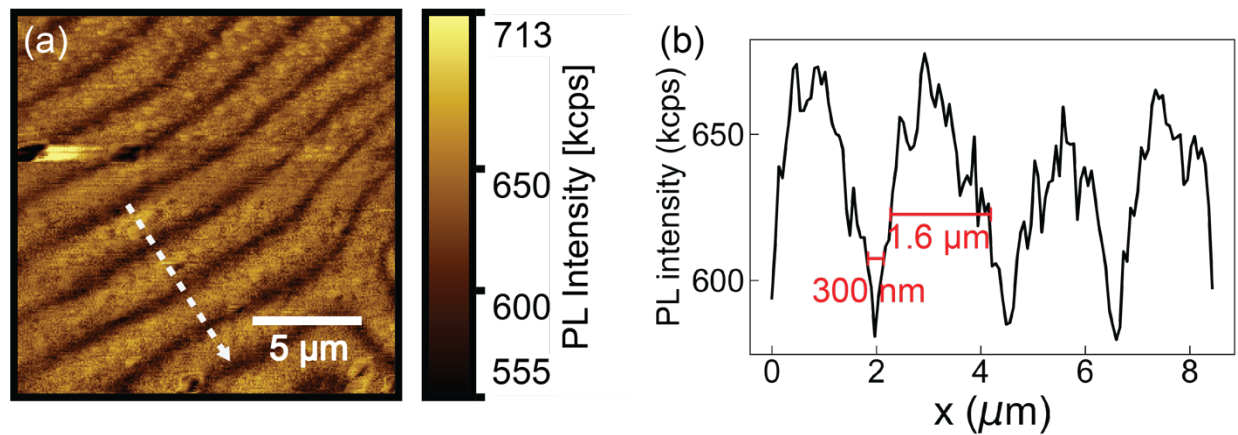


Fig. 4. (a) The diamond NV PL quenching image obtained as the probe was scanned over a $(\text{BiLu})_3\text{Fe}_5\text{O}_{12}$. The material's magnetic domain structure was observed because the NV spins felt high off-axis stray fields from the material. (b) Line-cut profile of the dashed line in (a).